TECHNICAL MEMORANDUM

398

The influence of physical processes on extratropical singular vectors

M.M. Coutinho[1], B.J. Hoskins[1] and R. Buizza

Research Department

[1]Department of Meteorology, University of Reading

Submitted to Journal of Atmospheric Sciences

April 2003

European Centre for Medium-Range Weather Forecasts
Europäisches Zentrum für mittelfristige Wettervorhersage
Centre européen pour les prévisions météorologiques à moyen terme

For additional copies please contact

The Library
ECMWF
Shinfield Park
Reading
RG2 9AX
library@ecmwf.int

Series: ECMWF Technical Memoranda

A full list of ECMWF Publications can be found on our web site under:
http://www.ecmwf.int/publications/

Abstract

An investigation is made of the impact of a full linearized physical (moist) parametrization package on extratropical singular vectors (SVs) using the ECMWF Integrated Forecasting System (IFS). Comparison is made for one particular period with a dry physical package including only vertical diffusion and surface drag. The crucial extra ingredient in the full package is found to be the large-scale latent heat release. Consistent with basic theory, its inclusion results in a shift to smaller horizontal scales and enhanced growth for the SVs. Whereas for the dry SVs T42 resolution is sufficient, the moist SVs require T63 to resolve their structure and growth. A 24h optimization time appears to be appropriate for the moist SVs because of the larger growth of moist SVs compared with dry SVs. Like dry SVs, moist SVs tend to occur in regions of high baroclinicity, but their location is also influenced by the availability of moisture. The most rapidly growing SVs appear to enhance or reduce large-scale rain in regions ahead of major cold fronts. The enhancement occurs in and ahead of a cyclonic perturbation and the reduction in and ahead of an anticyclonic perturbation. Most of the moist SVs for this situation are slightly modified versions of the dry SVs. However some occur in new locations and have particularly confined structures. The most rapidly growing SV is shown to exhibit quite linear behavior in the nonlinear model as it grows from 0.5 hPa to 12 hPa in one day. For five times this amplitude the structure is similar but the growth about half as the perturbation damps a PV trough or produces a cut-off, depending on its sign.

1 Introduction

As a complement to the normal mode theories of baroclinic instability for describing the growth of weather systems in the extra-tropical atmosphere, following an earlier suggestion by Lorenz (1965), Farrell (1982) and many subsequent studies have considered structures that are optimal for growth over a specific finite time interval. According to linear theory, given a specified norm and a linearized version of the prediction model and its adjoint, perturbations with optimal growth in a limited time interval can be calculated by a mathematical procedure described, for example, in Buizza and Palmer (1995). The resulting optimal perturbations are called singular vectors (SVs).

SVs are of both theoretical and practical interest. In the latter category, they are used by the European Centre for Medium-Range Forecasts (ECMWF) as a basis for giving a range of initial perturbations to an analysed state for their operational Ensemble Prediction System (EPS) (Molteni et al. 1996). In a linear sense, the forecasts from these perturbed initial conditions should give maximum divergence from the control forecast in an initial period.

The first SV studies considered linearized versions of filtered dynamical equations with no representation of other physical processes. Presently at ECMWF for the computation of SVs the dynamics are a linearization of that in the full forecast model and the physics consists only of a simple vertical diffusion and surface drag scheme. The latter was included to suppress shallow fast-growing structures near the surface that were considered to be not of interest since they were strongly damped in the nonlinear integrations (Buizza et al. 1993).

Hoskins et al. (2000) analysed the nature of the growth and structure of ECMWF extratropical SVs computed with such simplified physics. Particular aspects include an upscale energy transfer during SV development, generally a strong tilt against the shear in the initial structures, and a vertical distribution of energy, peaked in the lower to middle troposphere at the initial time and near tropopause and the surface at the final time (Hartmann et al. 1995). The geographical distribution of SVs was investigated, showing that structures typically developed moving from upstream and inside regions of maximum baroclinicity at the initial time to downstream of them at the final time. Thus, the upscale transfer of energy was suggested to be mostly a kinematic effect of the strengthening flow in the downstream direction.

The vertical structures were analysed by means of potential vorticity thinking in connection with the theoretical ideas on baroclinic initial value problems developed in Badger and Hoskins (2001). The vertical concentration

of the initial energy near a low-mid tropospheric level was related to the subsequent unshielding of opposite signed potential vorticity features by the action of the vertical shear in the zonal wind. The change in vertical structure during the growth process was explained by the propagation of westward tilted and eastward tilted Rossby waves forming the initial structure: the westward tilted structures grow and untilt as they propagate upwards whereas the eastward tilted structures decay and tilt more as they propagate downwards. The initial growth was explained as being an effect of the upward propagating Rossby wave only. A second, later period of sustained growth was explained in terms of the coupling of interior and boundary Rossby waves leading to normal mode-like growth. Therefore, short optimization times yield SVs that initially tend to be in the mid-troposphere (avoiding direct interaction with surface, that tends to inhibit the initial growth), whereas for longer optimization times the initial structures are lower (giving larger amplitude at the surface for coupling and more distance for upward propagation and growth). The time taken for the propagation to the tropopause and therefore the relevance of the coupling mechanism defines what was considered to be a short or a long optimization time.

The role of more complete physical processes in the perturbation growth mechanism can be taken into account using linearized models which include a more complete set of parametrizations. Ehrendorfer et al. (1999) studied the impact of the inclusion of moist physics on the computation of SVs using a linearized regional mesoscale model. They found that these SVs exhibited faster growth than those in the dry case and new structures appeared. At ECMWF, Mahfouf et al. (1996) found that the inclusion of large-scale condensation in the linearized calculation of T42 SVs resulted in larger amplification rates and smaller scales at the optimization time (48h). Mahfouf (1999) described a set of parametrizations developed for the linearized versions of the ECMWF global model. This more complete physics is used here and is presented in section 3. Barkmeijer et al. (2001) computed tropical SVs with such ECMWF physics, comparing the resulting positions and properties for different targeted areas in cases of tropical cyclones. In a companion paper, Puri et al. (2001) obtained a larger and more realistic spread in EPS forecast tropical cyclone tracks using perturbations based on targeted tropical SVs.

The motivation for this study is again both theoretical and practical. The impact of additional physical processes on baroclinic instability and weather system growth has been discussed since the work of Eady (1949). The largest impact might be expected from the inclusion of latent heat release and some of the deductions from the relevant theory are summarised here in section 2. It is of interest to see whether these ideas carry over to SVs. Pratically, it is necessary to understand whether important changes could be expected if the SVs for an ensemble of initial perturbations were determined in a much more expensive calculation that included a full parametrization package.

In section 3 of this paper the ECMWF linearized physics is briefly described and a range of experiments for one control forecast is defined. Section 4 describes and discusses the results and some concluding comments are given in section 5.

2 The impact of latent heat release on baroclinic instability and on the growth of weather systems

There are a number of complementary perspectives on the impact of large-scale latent heat release on mid-latitude weather system growth and behavior. Large-scale latent heat release occurs in the warm, moist air rising ahead of the surface low. The correlation between the positive temperature anomaly and the heating implies that the eddy available potential energy is increased. Latent heat release in convection at the cold front is less clear in this regard and convection in the cold air would act to reduce the available potential energy.

An alternative perspective on the impact of large-scale latent heat release is that the rising air follows a moist adiabat. The same can be true for the descending air if there is sufficient evaporation of falling precipitation

into it. As discussed in Hoskins (1987), arguments based on parcel displacements at half the steeper slope of moist adiabatic surfaces suggest that more perturbation energy will be obtained.

Following Bennets and Hoskins (1979), the relevance of the moist adiabat implies that there is reduced effective static stability, N, when the air is saturated. The Eady baroclinic instability model gives a growth rate maximum that is inversely proportional to N and a wavelength at which this occurs which is proportional to N. Therefore we expect that large-scale latent heat release will lead to increased growth rates and smaller wavelengths. In the Eady model the ageostrofic vertical circulation is proportional N^{-2} and can be expected to be enhanced for a given amplitude in the geostrofic fields. The measure of vertical instability in a semi-geostrophic model is the potential vorticity (PV). Emanuel et al. (1987) have used a semi-geostrophic model and represented the impact of latent heat release in the ascending air by reducing the effective PV to zero there. They found that the surface cyclone growth was enhanced by a factor of 2.5 and its horizontal scale was much reduced.

A reduced effective static stability due to latent heat release has similar implications in the initial value problems discussed in Badger and Hoskins (2001). In the Orr problem of a wave-like perturbation in a uniform sheared flow in an infinite domain the time-scale is proportional to N so that both growth and decay are enhanced. In the PV unshielding mechanism introduced by Badger and Hoskins (2001), if the initial state has PV anomalies of opposite signs situated in a vertical column then these cancel in their impact on the horizontal velocity field. However, under the action of a shear flow they separate, the cancellation reduces and the horizontal velocity field increases in magnitude. For the same initial PV anomalies but reduced N, the vertical scale for the velocity field associated with each anomaly is greater. Therefore the initial cancellation and the growth in the velocity field are larger. Also the vertical propagation of Rossby waves, another mechanism for development highlighted by Badger and Hoskins (2001), is increased for reduced N.

In a PV perspective, as discussed in Hoskins (1990), latent heat release leads to a positive PV tendency in the air below it and a negative tendency above. Since the lower tropospheric ascending air is less than a quarter wavelength ahead of the surface cyclone, an increase in the PV in this air due to large-scale latent heat release will act to increase the surface cyclonic circulation. Stoelinga (1996) has shown that this PV enhancement argument is applicable to the results he obtained from simulations with and without physical processes. In summary, the expectation from theory is that the addition of large-scale latent heat release, in particular, can be expected to give the possibility of initial perturbations that lead to considerably enhanced growth compared with the dry case. Also these initial perturbations will tend to have smaller horizontal scale.

3 Experimental set-up

The ECMWF improved linearized physics package (hereafter called full physics) includes representations of vertical diffusion, surface drag, gravity wave drag, large-scale condensation, long-wave radiation and deep cumulus convection. Mahfouf (1999) described the linearization of the parametrizations of these processes and showed that their inclusion results in a better agreement between the full nonlinear forecast model and the tangent-linear model. Here we give a summary of some aspects of the full physics schemes.

The formulation of the boundary layer is more complex than the simplified scheme (described in Buizza 1994b) included in the linearized models used for the optimization of SVs in Hoskins et al. (2000). The vertical diffusion is based on the use of exchange coefficients depending upon the local Richardson number as described in Louis et al. (1982). Analytical expressions are generalised for the situation of different roughness lengths for heat and momentum transfers. The mixing length profile of Blackadar (1962) is used, with a reduction in the free atmosphere.

The parametrization of large-scale condensation consists of a representation of stratiform precipitation in which local supersaturation is immediately removed by condensation and precipitation, taking into account the melting of snow. A full representation of the evaporation of precipitation in subsaturated layers was found by Mahfouf

(1999) to result in some undesirable SV characteristics, and so the effect was reduced compared with the nonlinear scheme. For convection a simplified mass-flux scheme, representing only deep convection, is used. Detrainment of cloud properties into the environment is neglected. The vertical transport of perturbed fields is estimated using mass-flux profiles obtained from a nonlinear integration of the convection scheme.

The various settings of physics, resolution and optimization time interval (OTI) of the experiments considered in this paper are listed in Table 1. The different settings of physics comprise: the full physics, a subset of the physics consisting only of vertical diffusion and surface drag - referred to as dry physics, and the individual inclusion of large-scale condensation or cumulus convection with the dry physics. An extratropical winter case starting from 17 February 1997 at 12 UTC is taken as the basic state for the experiments. This is the same basic state for which Hoskins et al. (2000) studied the behavior of dry SVs. A set of experiments is made using the same model resolution as in that paper, T42L31. However, as was discussed in section 2, the inclusion of moist processes may result in perturbations with smaller scales. Thus another set of experiments is performed using a finer resolution, T63L31.

Experiment Name	Physics Included	Resolution	OTI
D42-1	dry physics	T42L31	24h
F42-1	full physics	T42L31	24h
D42-2	dry physics	T42L31	48h
F42-2	full physics	T42L31	48h
D63-1	dry physics	T63L31	24h
F63-1	full physics	T63L31	24h
D63-2	dry physics	T63L31	48h
F63-2	full physics	T63L31	48h
Cond63-1	dry physics + large-scale condensation	T63L31	24h
Conv63-1	dry physics + cumulus convection	T63L31	24h

Table 1: Experiments

Another aspect of the experimental set-up is the horizontal diffusion used in the model. Buizza (1998) showed that growth rates and structures are affected by its specification. Here the diffusion is biharmonic and the T42 values are such as to give damping on the highest wavenumbers coefficients on time-scales of 15 h on temperature and vorticity and 6 h on divergence. At T63 resolution initial tests with equivalent time-scales 12 h and 4.8 h, respectively, exhibited computational noise in some SVs. This noise was not present when the diffusion was doubled. As a consequence, reduced time-scales of 6 h and 2.4 h, respectively, were used for all the calculations described in this paper.

Moist processes included in experiments with full physics allow the use of moisture during SV evolution, but initial humidity perturbations are not allowed in the experiments discussed here. The norm used in all these experiments is derived from a dry energy inner product as defined in Buizza and Palmer (1995), the so-called total energy norm. The optimal perturbations have unit norm at the initial time. They are constrained by a projection operator (Buizza 1994a) to have maximum amplitude at the final time in the region to the north of 30^oN. In most of the results, only the leading 10 SVs with the largest growth are considered. Further experiments using a norm that allowed initial moisture perturbations were made. The results are not considered here because, although SV amplification was larger, the structures found were very similar to the full physics structures computed using the dry norm.

4 Full physics effects on singular vectors

In this section the impact of the full physics on various characteristics of the SVs is analysed.

4.1 Amplification factors

As discussed in section 2, baroclinic growth in the presence of moist processes is expected to result in perturbations with larger growth rates. To explore this, Fig. 1 shows the amplifications factors for the ten leading SVs of experiments including either dry or full physics with resolutions T42 or T63 and OTIs of 24 or 48 hours. The amplification factors are defined as the ratio between the perturbation norm (that is the square root of the dry energy inner product) at the initial time and the perturbation norm at the final time, and correspond to the singular values of the forward tangent propagator.

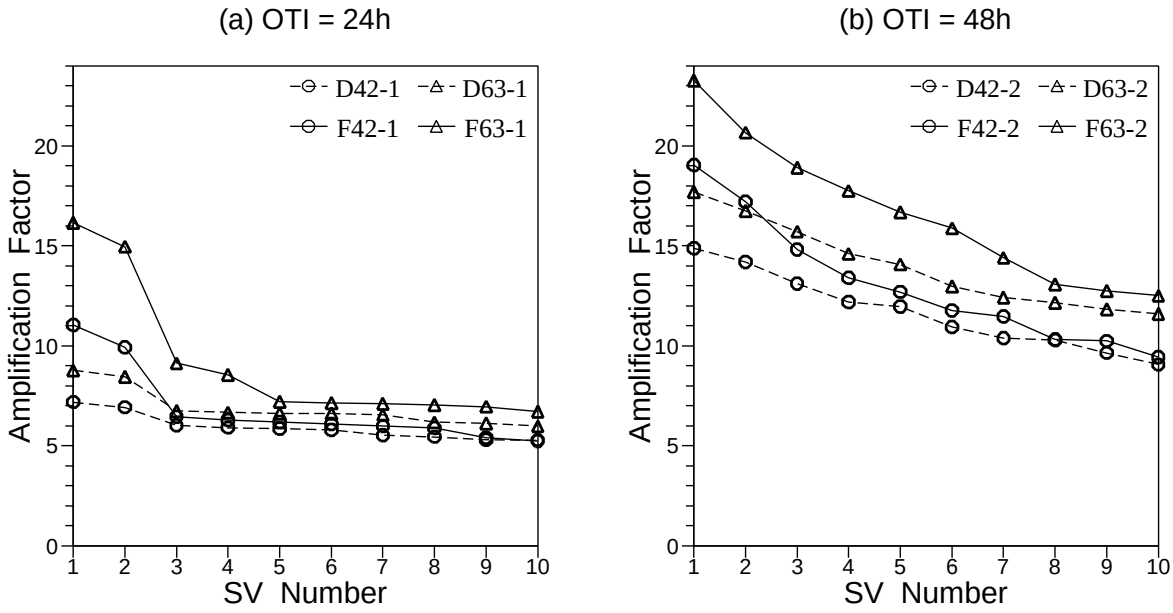

Figure 1: Amplification factors of the first ten SVs for experiments with dry physics (dashed lines) and full physics (solid lines) with truncation T42 (points denoted by ∘) and T63 (points denoted by △) and OTI of (a) 24h and (b) 48h.

For the experiments with OTI of 24h (Fig. 1 (a)), the amplification factors for the dry experiments decrease slightly from the first to the second SV and are smaller and nearly constant after that. The use of full physics results in further increase for SVs 1 and 2 in the experiment F42-1 and 1 to 4 in the experiment F63-1. Thus, the inclusion of diabatic processes significantly affects only the first few SVs that then become dominant. For OTIs of 48h (Fig. 1 (b)), the spectra of the dry amplification factors decrease more smoothly with increasing SV index. In contrast with the 24h experiments, the presence of diabatic processes in experiments F42-2 and F63-2 enhances the growth for all SVs. Larger growth rates for at least the first two SVs computed with full physics is a result found also in other cases to be discussed in a following paper. However, the increase in growth rate for all 48h SVs caused by diabatic processes is not a general result: in some situations larger growth occurs only for the first few SVs in 48h as well as in 24h OTIs.

As discussed in Badger and Hoskins (2001) and Hoskins et al. (2000), development in the initial growth period is more rapid than the more normal mode-like subsequent growth. This behavior is also found here. Thus, although SVs amplify many times their initial amplitudes in experiments with OTIs of 24h, the additional 24h

of growth in experiments with OTIs of 48h does not result in proportional additional amplification. For example, in the T63 full physics experiments the leading SV energy amplifies by a factor 16.2 over the 24h optimization interval, but the factor is only 1.4 times larger than this for the leading SV over the 48h optimization period.

48h SVs have also been determined for the period staring at 12 UTC on 16 February 1997 and finishing at the same time as that used for the 24h SVs. The amplification factor graphs are very similar to those for the overlapping but later period shown in Fig. 1 (b). However, the values are in general somewhat larger with, for example, the first SV giving factors 19.7 and 31.3 for the T63 dry and full physics computations, respectively.

The increase in the amplification factors when full physics is used is larger for experiments with truncation T63. For example, the maximum amplification factor increases from 7.2 to 11.0 going from D42-1 to F42-1, which corresponds to an increase of 53%. However in going from D63-1 to F63-1, it changes from 8.8 to 16.2, an increase of 84%. This result indicates the importance of the representation of smaller scales by the T63 truncation when moist processes are involved.

An alternative perspective on the relative amplification factors may be given by turning them into average doubling times. For the T63 experiments, these average doubling times for the first SV are 7.6h and 6.0h for the 24h OTI dry and full physics calculations. For the two 48h windows the doubling times are longer, corresponding to 11.6h and 11.2h, respectively, for the first dry SV and 10.6h and 9.7h for the first full physics SV.

Finally, it should be noted that the vertical diffusion scheme included in the improved physics package used here is damping more than the one used in Hoskins et al. (2000). SVs computed with the same resolution and OTI have amplification factors slightly reduced for the dry physics used here compared with the simplified scheme used there. This difference is approximately 10 percent for experiments with OTI of 48h and resolution T42. Mahfouf et al. (1996) also found smaller amplification factors for the improved vertical diffusion. However, there is no significant difference in the structure and general behavior between SVs computed with the old and the new boundary layer formulations.

4.2 Energy spectra

The mean total energy spectra for the first ten SVs for experiments with dry and full physics are shown in Fig. 2, for both the initial and the final time. At the initial time, the energy spectrum for SVs computed without moist processes is not significantly affected by increasing the horizontal resolution: the dry physics case spectra have similar shapes for both resolutions with both OTIs. The corresponding experiments including full physics have peaks at shorter wavelengths. This finding is in agreement with the effects of moist processes on baroclinic instability discussed in section 2. The shift to shorter wavelengths is much clearer for experiments with T63 resolution. For the T42 dry case the energy in the scales near the truncation at the initial time is significant and with the addition of moist processes these scales are not well resolved. Thus, when moist processes are included, the shift to smaller scales must be taken into account in the choice of resolution.

Comparing the spectra for the initial and the final time in Fig. 2, the upscale energy transfer during SV development is clear in all cases, but the physical processes present in the full physics experiments result in more total energy in smaller scales at the final time. Use of 24h rather than 48h as OTI results in less total energy at the final time, and with less time available for the upscale transport, more of this energy is associated with higher wavenumbers.

Because the T63 truncation permits better representation of the impact of the full physics processes in small scales, a clearer shift in the spectrum at the initial time when they are included and larger growth rates, it will be used from here onwards. Also, because the growth over the 48h OTI is not much larger than that over 24h and it is in the 24h OTI that the spectacular growth for full physics SVs is found (see section 4.a), we consider that a 24h OTI is more suitable for this study of full physics SV properties.

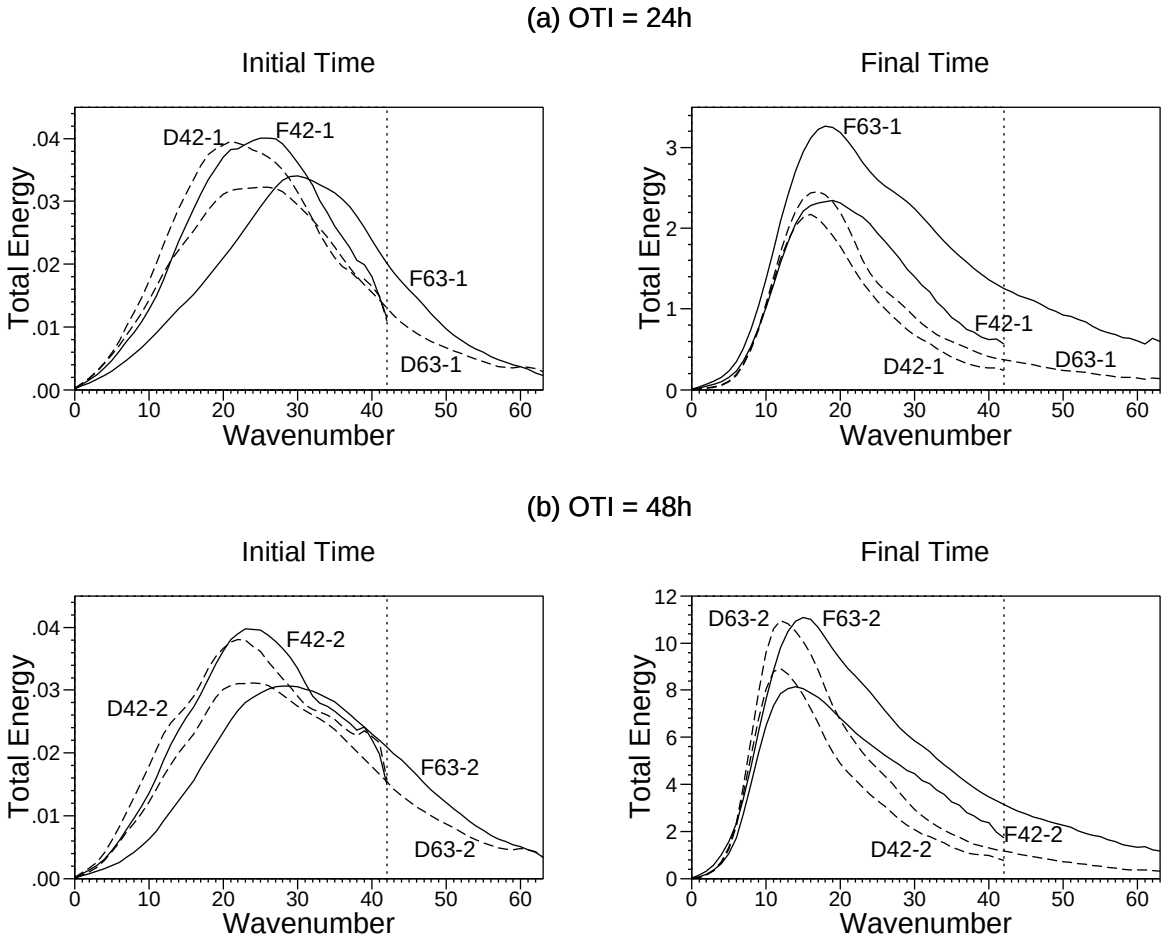

Figure 2: Spectral distribution of the total energy averaged for the first ten singular vectors as a function of total wavenumber for experiments with dry physics (dashed lines) and full physics (solid lines) at initial time (left) and final time (right) and OTI of (a) 24h and (b) 48h.

4.3 Total energy profile

The mean vertical distribution of total energy for the first ten SVs of experiments with resolution T63, 24h OTI and including dry or full physics is given in Fig. 3. The characteristic peaks in the lower to middle troposphere

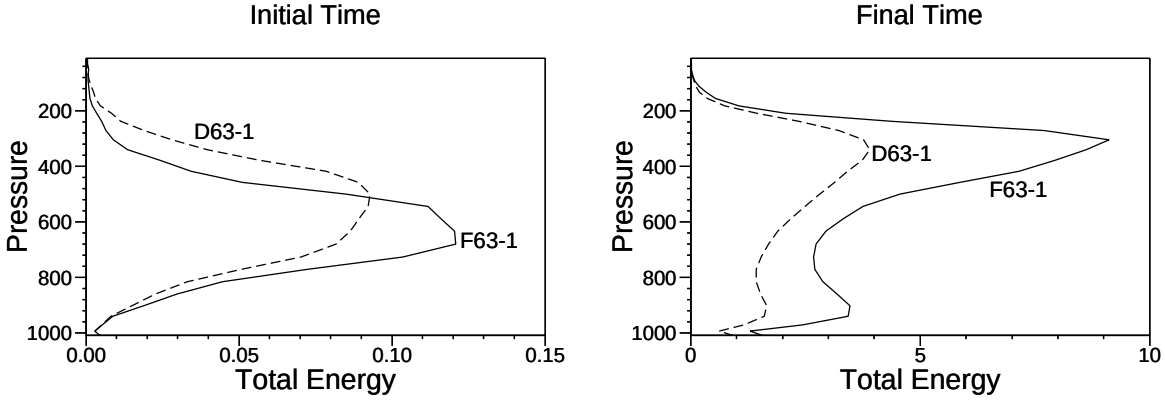

Figure 3: Total Energy averaged for the first ten SVs as a function of pressure for experiments D63-1 (dashed) and F63-1 (solid) at initial time (left) and final time (right).

at initial time and near the tropopause and the surface at the final time found by Hartmann et al. (1995) and Hoskins et al. (2000) for dry SVs are seen here for both experiments. For the full physics experiment, the average energy peak at the initial time is slightly lower and narrower.

As discussed in the introduction, during a first period of growth the energy of the initial perturbation increases as its westward tilted components propagate upwards. For the full physics experiments, larger growth is achieved due to the energy released by the diabatic processes, resulting in a pronounced final time energy peak observed at the tropopause.

4.4 Geographical distribution

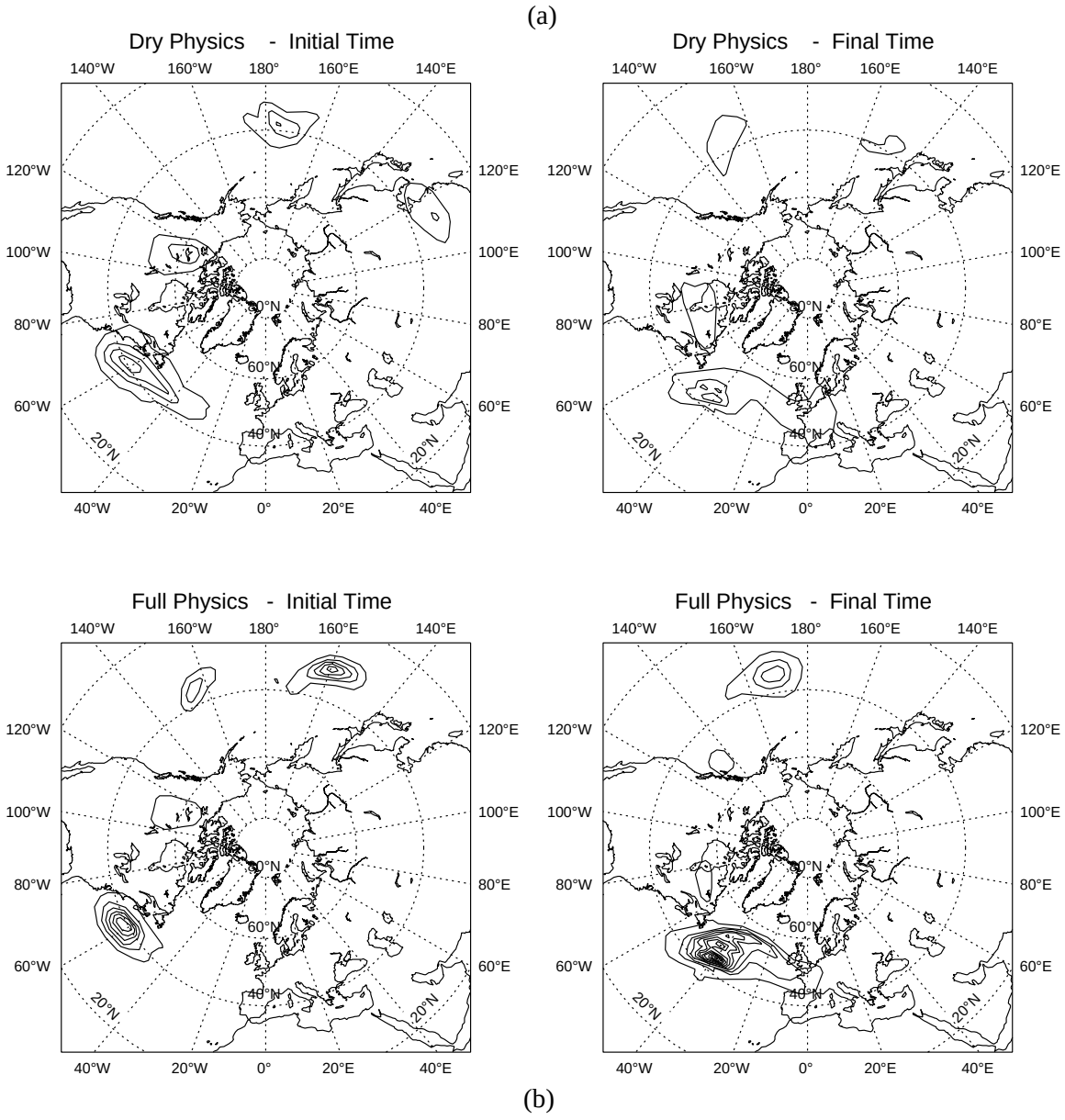

Figure 4: Geographical distribution of the amplification factor weighted energy of the first ten singular vectors at the initial time (left) and the final time (right) for (a) dry physics (D63-1) and (b) full physics (F63-1). The contour interval at the final time is 50 times that at the initial time.

Figure 4(a) shows the geographical distribution of the first ten SVs of experiment D63-1 at the initial and the

final times. The geographical distribution is evaluated as the vertically integrated amplification factor weighted sum of the kinetic and potential energy of the leading ten SVs. These distributions are in general consistent with the averaged baroclinicity index (Hoskins and Valdes 1990) shown in Fig. 5(a). As pointed out by Hoskins et al. (2000), the structures typically develop moving from upstream and inside regions of maximum baroclinicity at the initial time to downstream of them at the final time.

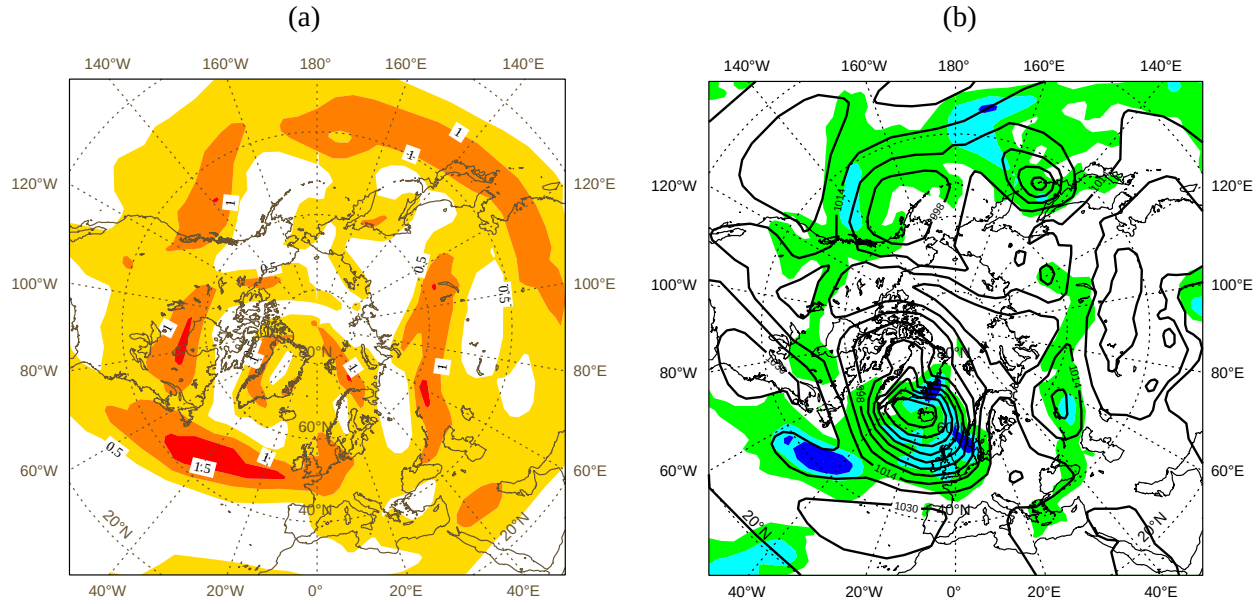

Figure 5: (a) 24h average baroclinicity index (17-18 Feb 12UTC). The contour interval is 0.5 d^{-1}. (b) 24h average mean sea level pressure (17-18 Feb 12UTC) and 24h forecast for 24h accumulated precipitation valid for 18 Feb 12UTC. The contour interval for pressure is 8hPa. Green colour corresponds to a precipitation range of 1-8mm, light blue to 8-16mm and dark blue to 16-36mm.

Compared with the dry experiment, the full physics experiment F63-1 shown in Fig. 4(b) has a very similar, although rather more concentrated, distribution over the Atlantic Ocean. In contrast, near the coast of Asia and over the Pacific Ocean the locations with full physics are displaced equatorwards and eastwards. The maximum in the initial energy near the coast of Asia in D63-1 moves from near 110^{o}E to near 160^{o}E in F63-1. In the Pacific the maximum moves from near the date-line in D63-1 to near 155^{o}W in F63-1. At the final time the distributions have moved downstream from the initial locations and the dominant regions over the Pacific Ocean are again localized further east for the full physics experiment. The maxima in the final energy changes from near 150^{o}E in D63-1 to near 165^{o}W in F63-1 and from near 155^{o}W in D63-1 to near 135^{o}W in F63-1.

Experiments Conv63-1 and Cond63-1, described in Table 1, were made to investigate the role of the two types of latent heat release in the changes observed for the full physics SVs. The geographical distributions for the first ten SVs in these two experiments are shown in Fig. 6. For experiment Conv63-1, the distribution given in Fig. 6(a) is very similar to that in Fig. 4(a), for D63-1. In contrast, the distribution shown in Fig. 6(b) for the experiment Cond63-1, with its similarity to Fig. 4(b), for F63-1, indicates that the large-scale condensation is the physical parametrization responsible for the displacement of the SVs in the Pacific Ocean region observed in the full physics experiment. Further investigation shows that the amplification factors and structures of the individual SVs are indeed very similar to those with the full physics package.

The similarity between the SVs in various experiments may be quantified by the computation of the similarity index described in Buizza (1994b) as the mean of the projection coefficients of the SVs of one experiment on the SVs of the other experiment. Table 2 shows the similarity indices for the first 15 SVs of T63 24h OTI experiments with different physical processes. These indices indicate that D63-1/Conv63-1 and F63-1/Cond63-1 have a high degree of similarity (similarity indices greater than 0.85). On the other hand, experiments

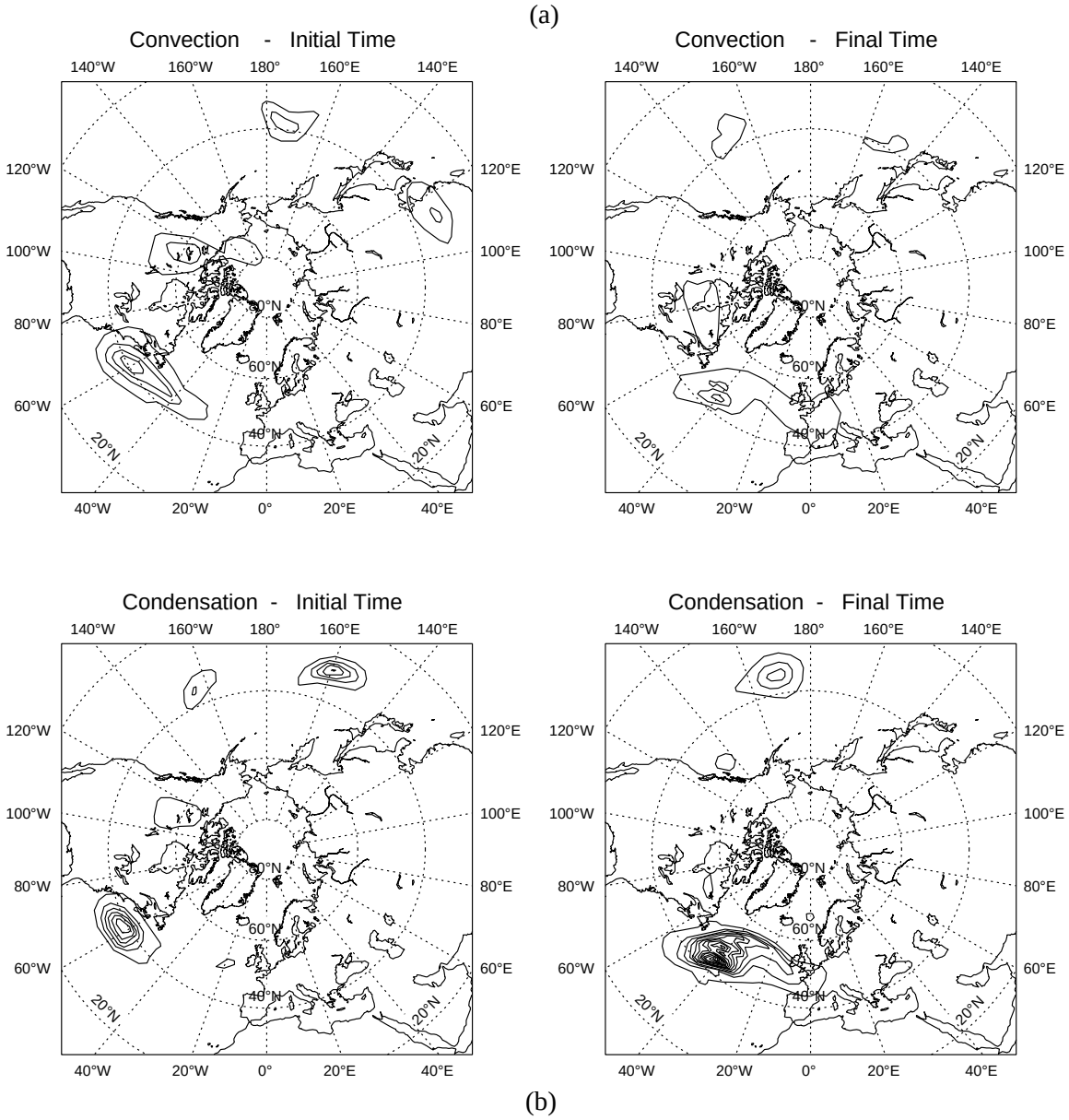

Figure 6: Same as Fig. 4, but for experiments (a) Conv63-1 and (b) Cond63-1. The contour interval at the final time is 50 times that at the initial time.

D63-1/Cond63-1 and F63-1/Conv63-1 have similarity indices of about 0.50. For some of the 15 SVs of D63-1 or F63-1 the sum of the projection coefficients (not shown) on the first 15 SVs of Cond63-1 or Conv63-1, respectively, is less than 0.10.

Similarity	D63-1	F63-1	Cond63-1	Conv63-1
D63-1	1.00	0.54	0.54	0.86
F63-1		1.00	0.87	0.54
Cond63-1			1.00	0.51
Conv63-1				1.00

Table 2: Similarity indices between the various T63 24h OTI experiments calculated using the 15 leading SVs.

Figure 7 gives the distributions at initial and final times of the SVs shown in Fig. 4(b), superimposed on the basic state total column water vapour content at the same times. This shows clearly that, although the distributions of the full physics SVs over the Pacific Ocean are still over regions of high baroclinicity (c.f. Fig. 5(a)), their exact positions are displaced towards the local maxima in moisture at both the initial and the final times. SVs calculated using 48h OTI are found to exhibit very similar behavior (not shown). Examination of the synoptic situation, e.g. Fig. 5(b), indicates that the full physics SVs tend to exist in and move along the precipitation regions ahead of cold fronts. The total precipitation shown in Fig 5(b) is dominated by large-scale rain. It appears that the SVs use the modification of the latent heat release in the large-scale rain there to enhance their growth. This hypothesis will be considered further in the next section.

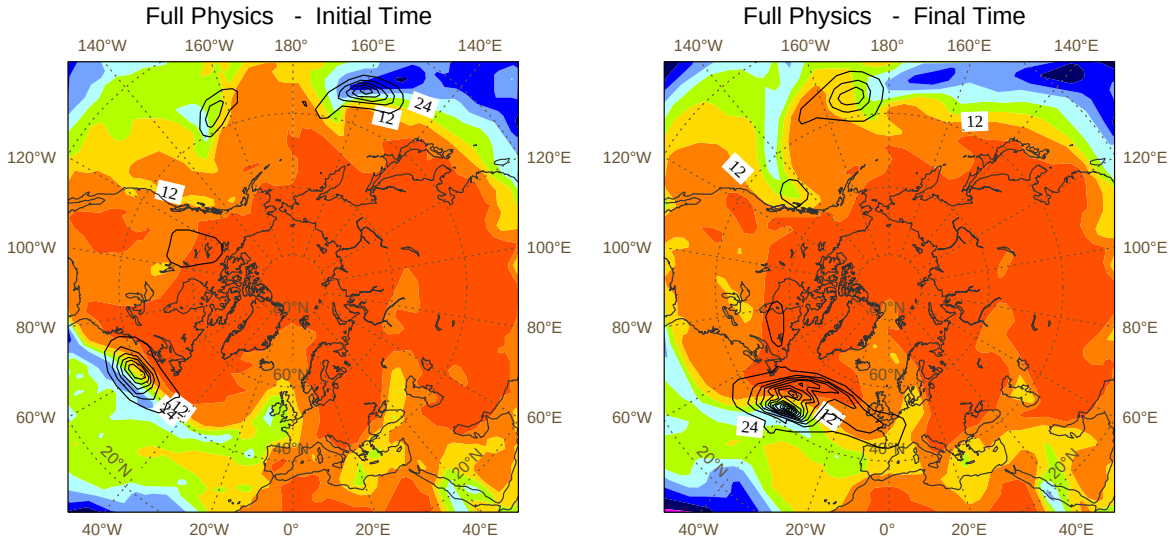

Figure 7: Fig. 4(b) superimposed on the basic state total column water vapour (TCWV) content at the initial time (left) and the final time (right). The contour interval for TCWV is 6 kg m^{-2}.

The different impact of full physics for SVs over the Asia/Pacific region compared to the Atlantic region is consistent with the fact that in the Atlantic the region where the dry SVs are concentrated is also a region of large water vapour availability, thus, the SVs do not move when moist processes are included.

4.5 Moist mechanisms for growth

Having found that inclusion of full physics, and in particular large-scale latent heat release, results in larger growth for all SVs and change in some SV locations, moist SV structures and mechanisms for growth are investigated in this section. To determine the PV perturbation associated with an SV, the contribution of the PV of the basic state is subtracted from the PV of the perturbed state. The vertical derivatives in the PV computation are calculated using a centred finite difference scheme in the interior and forward and backward differences at the boundaries.

Figure 8 (a) and (b) show longitude height sections of streamfunction for the first SV of experiments D63-1 and F63-1 at the initial and final times. In both experiments, this dominant SV has a similar location, starting on the coast of North America and evolving over the Atlantic Ocean. As seen in Fig. 8, the full physics SV has slightly smaller scale and larger final amplitude, but the structures are similar in the two cases. The corresponding PV sections in Fig. 8 (c) and (d) show tight westward tilted initial structures, tilting into the vertical during the growth process, with a large final amplitude near the surface.

The second SVs of experiments D63-1 and F63-1 (not shown), also near the coast of North America are similar to the corresponding SV1 but shifted by approximately a quarter wavelength. In fact, apart from moist SVs

at new locations in the Pacific Ocean discussed in section 4.d, moist SV structures closely resemble the dry structures, and the main difference is that their growth is enhanced by latent heat release.

(a) Streamfunction D63-1

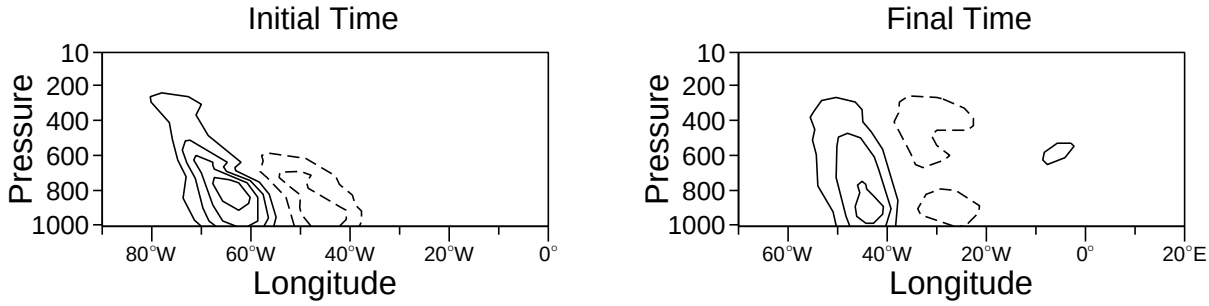

(b) Streamfunction F63-1

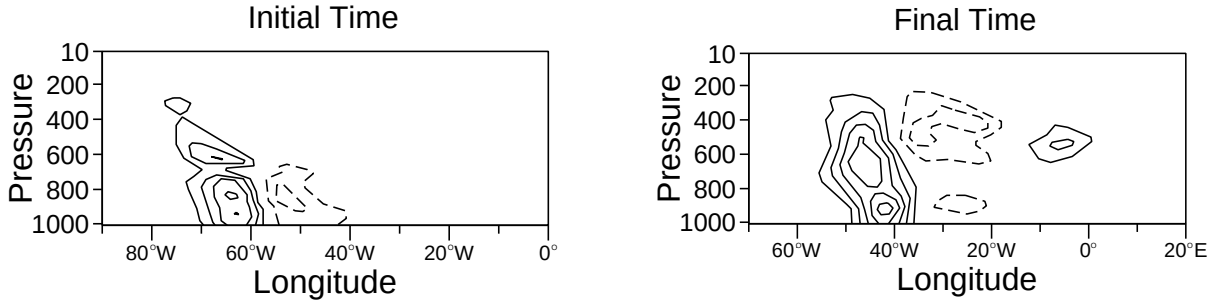

(c) PV D63-1

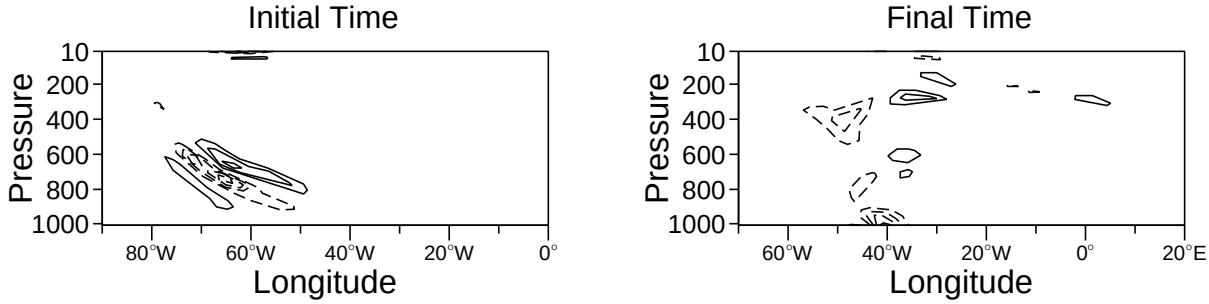

(d) PV F63-1

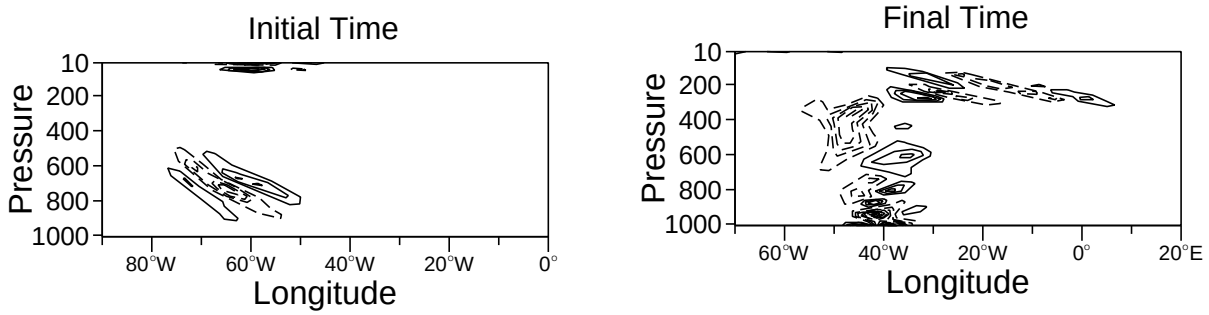

Figure 8: Longitude-pressure cross-sections for the first singular vectors, at the initial (left) and final (right) times, of (a) streamfunction for D63-1, (b) streamfunction for F63-1, (c) PV for D63-1 and (d) PV for F63-1. Initial time at 40°N and final time at 44°N. The streamfunction contour at the final time is 20 times that at the initial time and the PV contour at the final time is 5 times that at the initial time.

In contrast, the third SV of F63-1 is in a region that was not selected as optimal by the original set of dry SVs. It is the largest growth SV localized in the West Pacific region. Figure 9 shows longitude height sections for the third F63-1 SV and for the eighth D63-1 SV, the one with the largest growth localized in Asia/West Pacific.

(a) Streamfunction D63-1

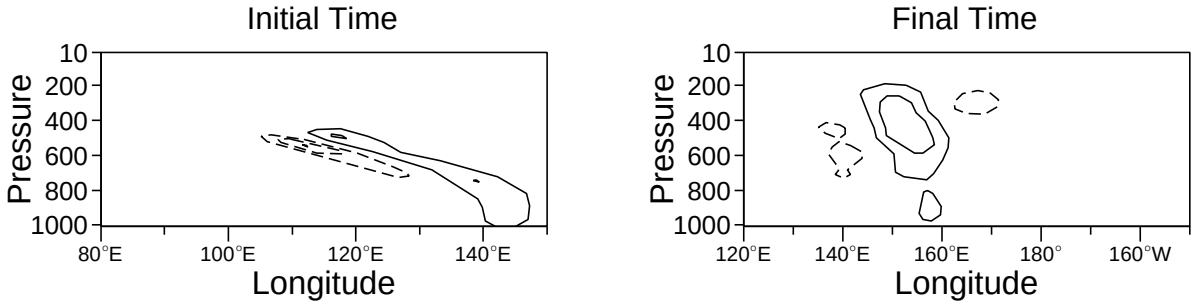

(b) Streamfunction F63-1

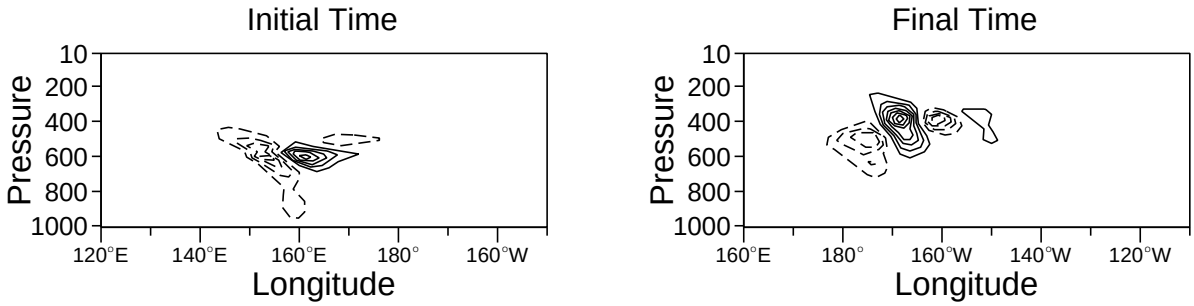

(c) PV D63-1

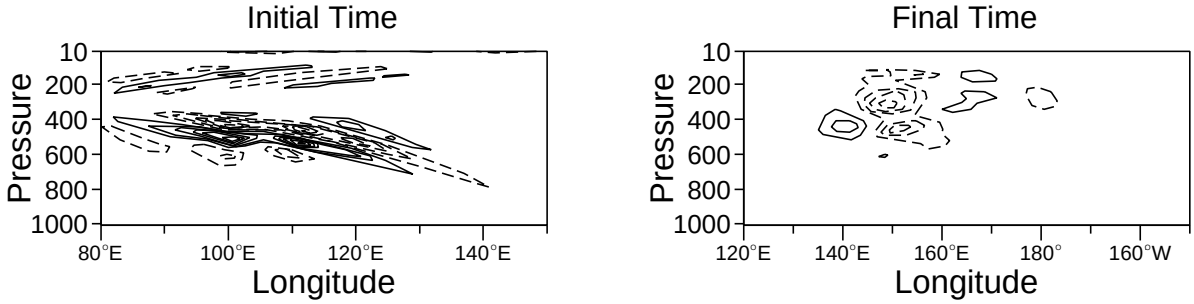

(d) PV F63-1

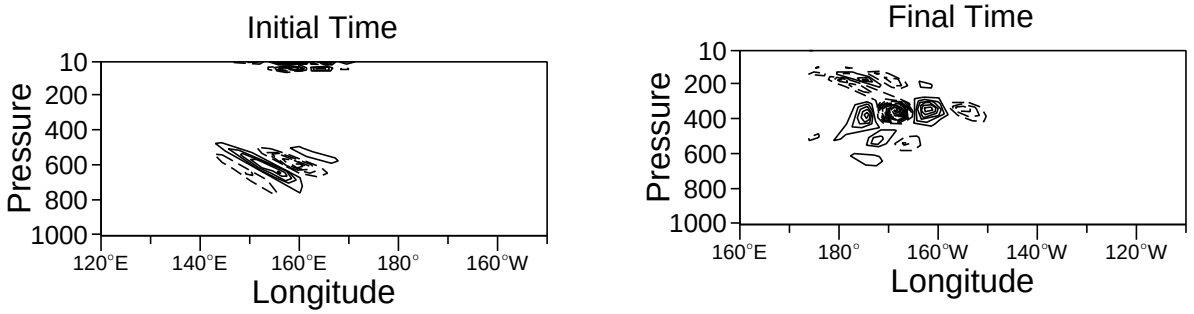

Figure 9: Same as Fig. 8, but for the eighth singular vector of D63-1 and the third singular vector of F63-1. Initial time at 33°N for (a) and (c) and 31°N for (b) and (d). Final time at 36°N for (a) and (c) and 35°N for (b) and (d). The streamfunction and PV contours are the same as in Fig. 8.

Clearly, the moist SV has a tighter structure, very concentrated in the vertical, and quite different from all dry ones. The sum of the projection coefficients of SV3 of F63-1 on the first 15 SVs of D63-1 is only 0.08. In contrast, for the first SV of F63-1 this sum is 0.72, and the projection coefficient on SV1 of D63-1 is 0.66.

As shown in Fig. 9, the third moist SV has a westward tilt at the initial time that is not completely lost at the final time. It has a very organized structure that resembles the ones discussed in Badger and Hoskins (2001). In this case, as represented by the model, large-scale condensation is the crucial ingredient responsible for creating an optimal structure in that region. In contrast to the first and the second moist SVs, this third SV clearly depends strongly on the availability of moisture. Its very tight structure can be explained, as discussed in section 2, by a reduction in the effective static stability associated with latent heat release. Consistent with basic theory this enhances growth and upward propagation. Thus, although the mechanism for growth is the same as for the other SVs, the existence of this SV is considerably influenced by the reduced effective static stability.

In addition to baroclinic mechanisms, barotropic mechanisms of SV growth have also been discussed, for example, in Buizza and Palmer (1995). This conversion of kinetic energy from the basic state to the perturbations is indicated by initial SV tilts against the horizontal shear. In general, the moist structures show less evidence of such a tilt and therefore of barotropic conversion.

Precipitation changes associated with a particular SV were most easily obtained from integrations with the full forecast model. The initial time SV was added with either sign to the control state at the initial time with an amplitude, 0.25 hPa maximum surface pressure amplitude, such that its evolution should be linear for one day. The perturbation evolution was obtained by subtracting the control forecast from the perturbed forecast at corresponding times. The resulting 24h surface pressure and 21-24h accumulated precipitation changes for a full physics SV 1, with the initial sign being such that its structure is dominated by a cyclone, are shown in Fig. 10(a). Also indicated by an 'L' is the initial position of the surface low. Taking account of the movement of the system it is clear that precipitation is enhanced in and ahead of the perturbation surface low, consistent with expectations. The reduction of precipitation on the southern flank of the low could be associated with bringing cooler, drier air into this region.

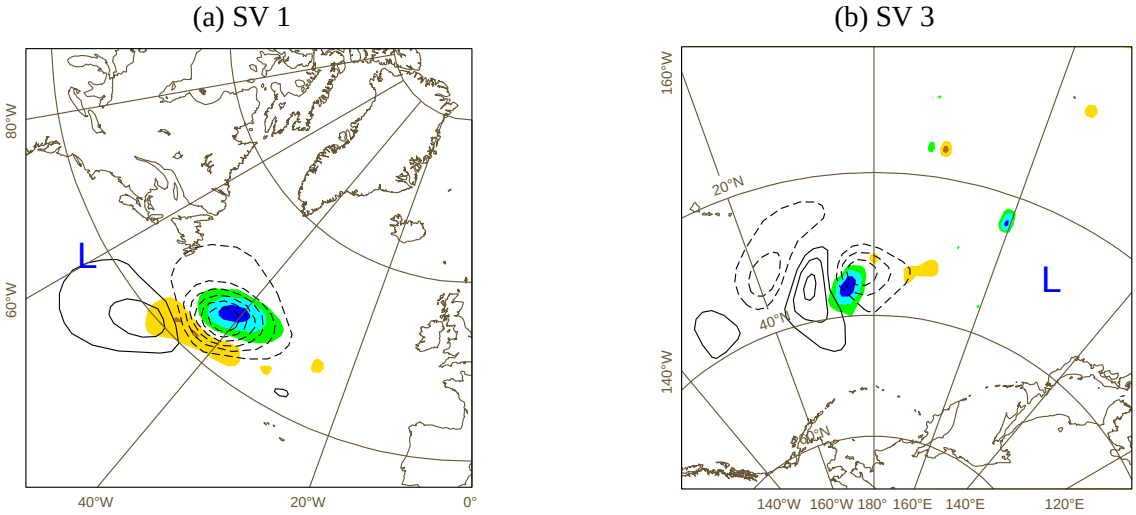

Figure 10: Differences derived from nonlinear integrations initialised with the analysed state perturbed by small amplitude full physics SVs: (a) 21-24h accumulated precipitation (shaded) and 24h mean sea level pressure (contours) for SV 1 and (b) 21-24h accumulated precipitation (shaded) and 500hPa streamfunction (contours) for SV 3. In (a), the contour interval for pressure is 1hPa and the contours are drawn at ±0.5hPa, ±1.5hPa, etc. Accumulated precipitation anomalies greater than 0.5mm, 1.5mm and 2.5mm are shown by green, blue and dark blue colours, respectively. Anomalies less than -0.5mm and -1.5mm are shown by yellow and brown colours, respectively. L indicates the position of the surface low at the initial time. In (b) the contour interval is $0.2m^2s^{-1}$ for streamfunction and 0.2mm for precipitation. L indicates the initial position of the cyclone.

Figure 10(b) shows a similar figure for SV 3 but using 500 hPa streamfunction because of the small amplitudes near the surface. There is clearly enhancement of precipitation ahead of the low and suppression behind it.

Comparing with Fig. 5(b) it is seen that SV 1 and SV 3 are associated with enhancement and reduction of the precipitation in different parts of the two major cold front precipitation regions near 45^{o}W and 180^{o}E, respectively.

4.6 Nonlinear behavior

In the previous section, we have referred to results of nonlinear integrations to investigate the precipitation changes with respect to the perturbation growth. A further purpose of nonlinear experiments is to explore the limitations of the linear theory in the moist case. Therefore, perturbations with amplitudes corresponding to 2

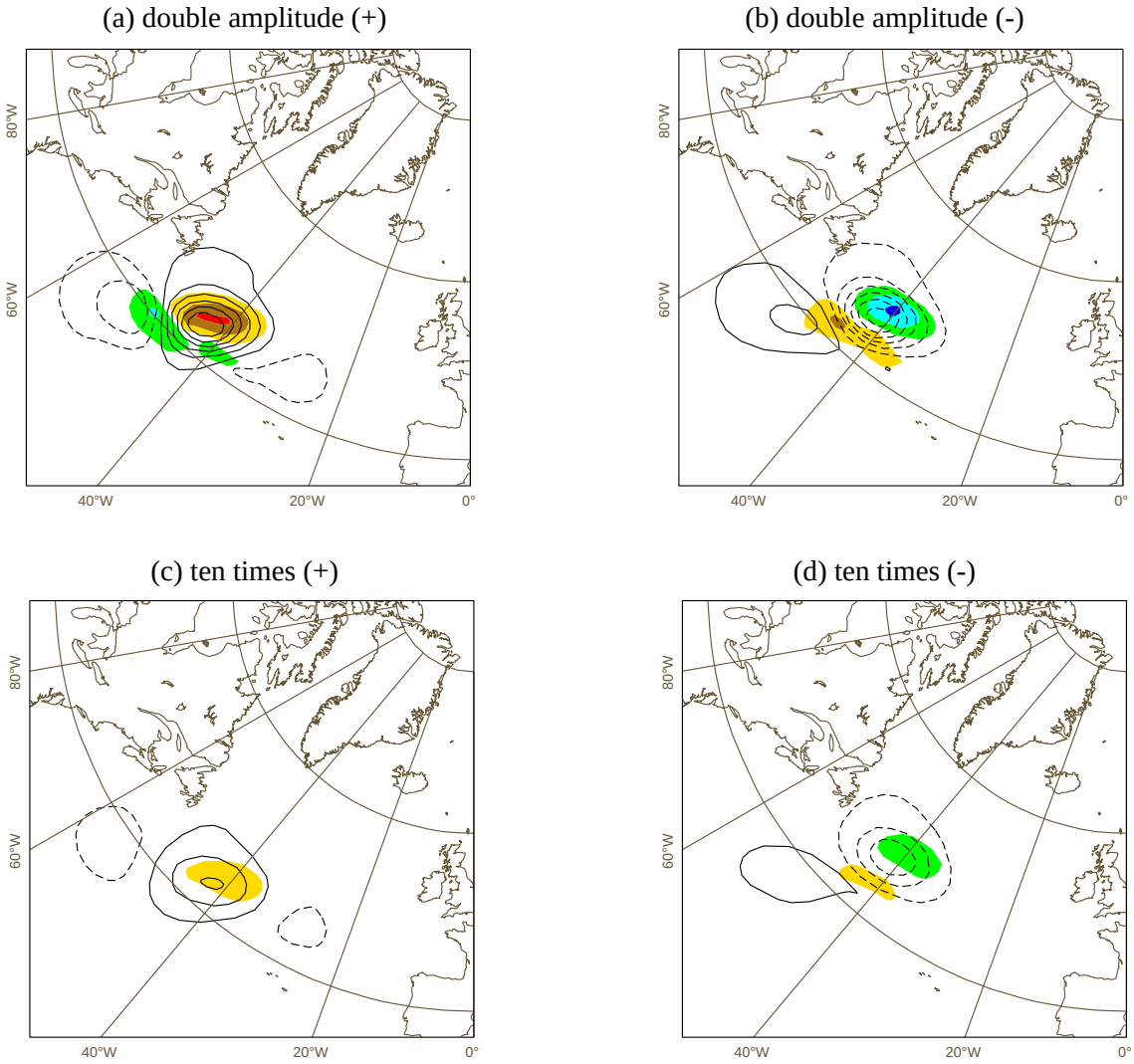

Figure 11: 21-24h accumulated precipitation and 24h mean sea level pressure differences derived from nonlinear integrations initialised with the analysed state perturbed by full physics SV 1 with amplified initial amplitude relatively to section 4.e: (a) positive 2 times, (b) negative 2 times, (c) positive 10 times and (d) negative 10 times. The contour interval in (a) and (b) is 2hPa for pressure and 2mm for precipitation (twice that in Fig. 10 (a)) and in (c) and (d) 10hPa and 10mm (ten times that in Fig. 10 (a)), so that linear behavior would make each picture the same as that in Fig. 10 (a) (with reversed sign for (a) and (c)).

and 10 times the initial perturbation used in section 4.e were added to the control state at initial time and the resulting perturbed initial conditions were integrated for 24h.

The maximum surface pressure amplitude for the full physics SV 1 in the full model discussed in section 4.e was 0.25 hPa at the initial time and 6 hPa at the final time. Both the factor 24 in the growth of the surface low and the 24h structure of the surface pressure field were very similar to that given by the SV obtained from the linear model. For positive and negative full physics SV 1 with the larger amplitudes the resulting 24h surface pressure and 21-24h accumulated precipitation changes are shown in Fig. 11. The final maximum amplitude for the perturbations corresponding to twice the initial amplitude in section 4.e is approximately 12 hPa, twice as much as that obtained there. Also, consistent with linear behavior, the positive and negative perturbations have similar behavior. However, for the largest amplitude the initial surface pressure maximum is 2.5 hPa and the final maximum amplitude is about 30 hPa, instead of the value 60 hPa implied by linear behavior. This implies that nonlinearity, as expected, is significant for this amplitude. However the structure at 24h for both positive and negative perturbations is still similar to that for smaller amplitudes.

The anticorrelation between evolved positive and negative perturbations, computed as described in Buizza (1995), supports these conclusions. The anticorrelation is 0.86 and 0.80 for the first two amplitudes, while for the largest SV amplitude the anticorrelation is 0.60. Also, the relative nonlinearity index of

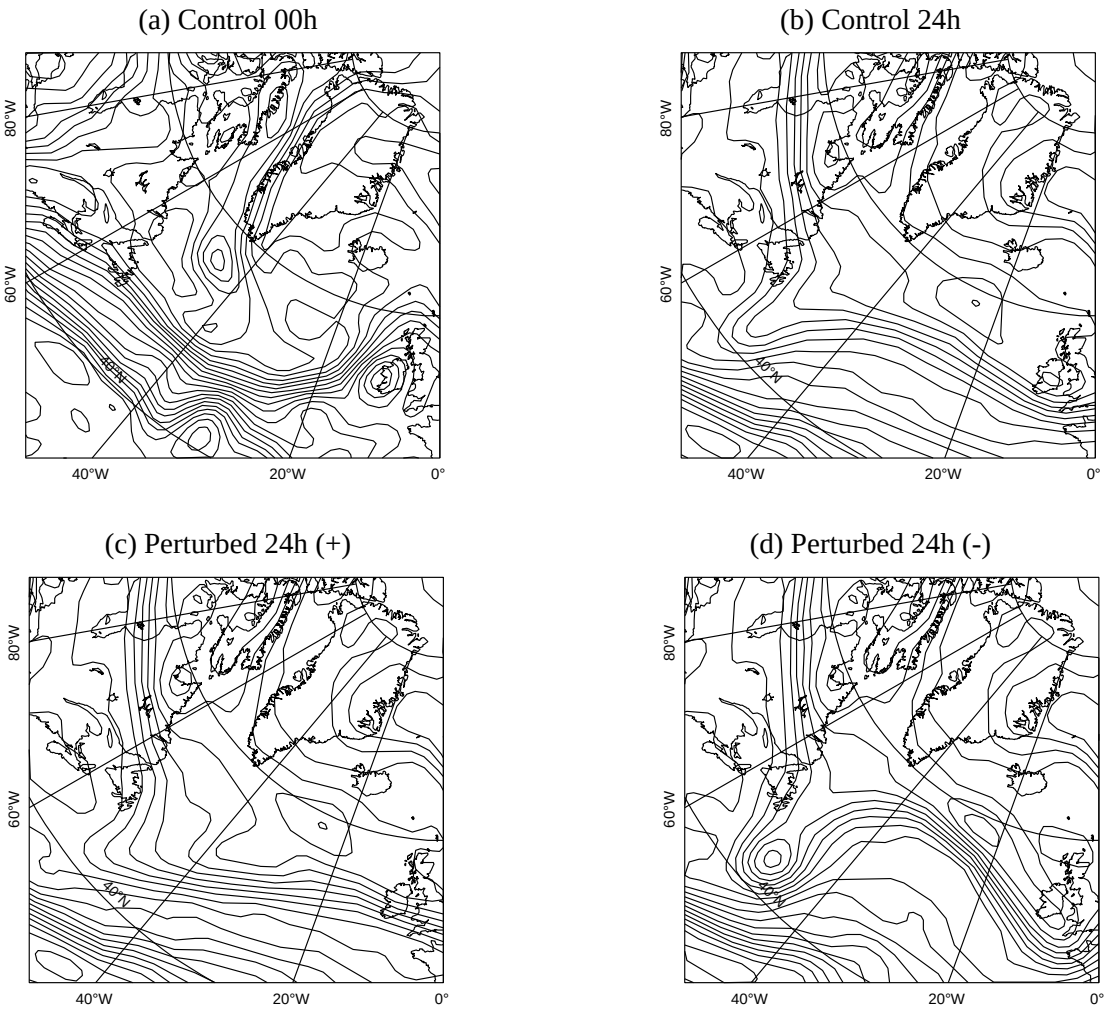

Figure 12: θ on the PV=2 surface for (a) the control analysis, (b) the control forecast at the final time and the two final perturbed forecasts with the largest amplitude perturbation obtained from the first moist SV with (c) positive sign and (d) negative sign. The contour interval is 5K.

Gilmour et al. (2001) increases from 0.53 and 0.65 for the first two amplitudes to 0.94 for the largest amplitude.

To further explore the nonlinear behavior for the largest amplitude, Fig. 12 shows potential temperature, θ, on the PV=2 surface for the control analysis, the control forecast at the final time and the two final perturbed forecasts with the largest amplitude perturbation obtained from the first full physics SV. In the control run, a trough propagates from the east coast of North America over the western North Atlantic. In the final forecast generated from the larger negative perturbation, seen in Fig. 12(d), the tip of the trough has already started to cut off and a strong downstream ridge has developed. An opposite behavior is seen in the forecast obtained from the positive perturbation (Fig. 12(c)): the trough is less pronounced and the ridge is not present. The large amplitude changes and, in particular, the cut-off dynamics in the negative perturbation case are consistent with the breakdown of linearity in this case.

5 Conclusions

In this paper it has been shown using the ECMWF IFS that physical processes have an important impact on SV growth and structure.

In agreement with previous understanding of the effects of moist processes on baroclinic instability, enhanced growth rates and shorter wavelengths have been found. Consistent with these changes, it has been shown that when moist processes are considered a T63 truncation, rather than T42, is more appropriate and a 24h OTI is more suitable than the 48h usually used for dry SVs.

Both dry and full physics SVs tend to be concentrated in regions of high baroclinicity, but the exact locations of full physics SVs are also influenced by the availability of moisture. It has been found that the parametrization of large-scale condensation is the dominant process in the full physics package and is responsible for nearly all the impact of full physics on extratropical SVs. The parametrizations of gravity wave drag, long wave radiation and deep cumulus convection appear to have little influence on extratropical SVs.

Most of the moist SVs analysed are slightly modified versions of the dry SVs. However some occur at new locations and have tighter structures, very concentrated in the vertical. This result is consistent with results from Ehrendorfer et al. (1999), where some of the SVs resulting from the use of moist physics were new compared to the dry case, whereas others were similar.

As in the dry case, growth may be explained as in Hoskins et al. (2000) by PV unshielding, upward propagation and coupling of waves, but now facilitated by energy release from large-scale condensation. The most rapidly growing SVs enhance or reduce precipitation in regions ahead of major cold fronts. A cyclonic perturbation results in enhancement of the rain in and ahead of it whereas reduction occurs in and ahead of an anticyclonic perturbation.

In practical applications of moist SVs, such as ensemble prediction, the linearity assumption must be valid for perturbations of reasonable amplitude, comparable to the size of typical uncertainties (Errico and Raeder, 1999). The most rapidly growing SV here has a linear behavior in the nonlinear model as it grows from 0.5 hPa to 12 hPa in 24h. For five times this amplitude the structure is similar but the amplitude reached is about half that given by linear theory. A perturbation with this amplitude can change the flow by damping a trough or sharpening it and producing a cut-off, depending on its sign, indicating an earlier breakdown of the linearity approximation.

Moist processes are particularly important in perturbation growth in severe storm cases. A study of the impact in a range of such cases will be reported in a subsequent paper.

Acknowledgements

We wish to thank Tim Palmer and anonymous referees for helpful comments. M.M.Coutinho was supported by the Brazilian Agency CAPES process 1329/98-7.

References

Badger, J. and Hoskins, B. J., 2001: Simple initial value problems and mechanisms for baroclinic growth. *J. Atmos. Sci.*, **58**, 38-49.

Barkmeijer, J., Buizza, R., Palmer, T. N., Puri, K. and Mahfouf, J.-F., 2001: Tropical singular vectors computed with linearised diabatic physics. *Quart. J. Roy. Meteor. Soc.*, **127**, 685-708.

Bennets, D. A. and Hoskins, B. J., 1979: Conditional symmetric instability - a possible explanation for frontal rainbands. *Quart. J. Roy. Meteor. Soc.*, **105**, 945-962.

Blackadar, A. K., 1962: The vertical distribution of wind and turbulent exchange in a neutral atmosphere. *J. Geophys. Res.*, **67**, 3095-3102.

Buizza, R., 1994a: Localization of optimal perturbations using a local projection operator. *Quart. J. Roy. Meteor. Soc.*, **120**, 1647-1681.

Buizza, R., 1994b: Sensitivity of optimal unstable structures. *Quart. J. Roy. Meteor. Soc.*, **120**, 429-451.

Buizza, R., 1995: Optimal perturbation time evolution and sensitivity of ensemble prediction to perturbation amplitude. *Quart. J. Roy. Meteor. Soc.*, **121**, 1705-1738.

Buizza, R., 1998: Impact of horizontal diffusion on T21, T42, and T63 singular vectors. *J. Atmos. Sci.*, **55**, 1069-1083.

Buizza, R. and Palmer, T. N., 1995: The singular-vector structure of the atmospheric global circulation. *J. Atmos. Sci.*, **52**, 1434-1456.

Buizza, R., Tribbia, J., Molteni, F. and Palmer, T., 1993: Computation of optimal unstable structures for a numerical weather prediction model. *Tellus*, **45A**, 388-407.

Eady, E. T., 1949: Long waves and cyclone waves. *Tellus*, **1**, No.3, 33-52.

Ehrendorfer, M., Errico, R. M. and Raeder, K. D., 1999: Singular-vector perturbation growth in a primitive equation model with moist physics. *J. Atmos. Sci.*, **56**, 1627-1648.

Emanuel, K., Fantini, M. and Thorpe, A., 1987: Baroclinic instability in an environment of small stability to slantwise moist convection. Part I: two-dimensional models. *J. Atmos. Sci.*, **44**, 1559-1573.

Errico, R. M. and Raeder, K. D.,1999: An examination of the accuracy of the linearization of a mesoscale model with moist physics. *Quart. J. Roy. Meteor. Soc.*, **125**, 169-195.

Farrell, B. F., 1982: The initial growth of disturbances in a baroclinic flow. *J. Atmos. Sci.*, **39**, 1663-1686.

Gilmour, I., Smith, L. A. and Buizza, R., 2001: Linear regime duration: Is 24 hours a long time in synoptic weather forecasting? *J. Atmos. Sci.*, **58**, 3525-3539.

Hartmann, D. L., Buizza, R. and Palmer, T. N., 1995: Singular vectors: the effect of spatial scale on linear growth of disturbances. *J. Atmos. Sci.*, **52**, 3885-3894.

Hoskins, B. J., 1987: Theories of cyclogenesis. *ECMWF Seminar on the nature and prediction of extra tropical*

weather systems, Shinfield Park, Reading, U.K., ECMWF, 1-15.

Hoskins, B. J., 1990: Theory of Extratropical Cyclones. *Extratropical Cyclones, The Erik Palmén Memorial Volume*, C. W. Newton and E. O. Holopainen, Eds., Amer. Meteor. Soc., 63-80.

Hoskins, B. J. and Valdes, P. J., 1990: On the existence of storm tracks. *J. Atmos. Sci.*, **47**, 1854-1864.

Hoskins, B. J., Buizza, R. and Badger, J., 2000: The nature of singular growth and structure. *Quart. J. Roy. Meteor. Soc.*, **126**, 1565-1580.

Lorenz, E. N., 1965: A study of the predictability of a 28-variable atmospheric model. *Tellus*, **17**, 321-333.

Louis, J.-F., Tiedtke, M. and Geleyn, J.-F., 1982: A short history of the operational PBL parametrization at ECMWF. *ECMWF Workshop on boundary layer parametrization*, Shinfield Park, Reading, U.K., ECMWF, 59-79.

Mahfouf, J.-F., 1999: Influence of physical processes on the tangent linear-approximation. *Tellus*, **51A**, 147-166.

Mahfouf, J.-F., Buizza, R. and Errico, R. M., 1996: Strategy for including physical processes in the ECMWF variational data assimilation system. *ECMWF Workshop on non-linear aspects of data assimilation*, Shinfield Park, Reading, U.K., ECMWF, 595-632.

Molteni, F., Buizza, R., Palmer, T. N., and Petroliagis, T., 1996: The ECMWF ensemble prediction system: Methodology and validation. *Quart. J. Roy. Meteor. Soc.*, **122**, 73-119.

Puri, K., Barkmeijer, J. and Palmer, T. N., 2001: Ensemble prediction of tropical cyclones using target diabatic singular vectors. *Quart. J. Roy. Meteor. Soc.*, **127**, 709-731.

Stoelinga, M. T., 1996: A potential vorticity-based study of the role of diabatic heating and friction in a numerically simulated baroclinic cyclone. *Mo. Wea. Rev.*, **124**, 849-874.